minerals

MDPI

Article

Spatial and Temporal Evolution of Groundwater Chemistry of Baotu Karst Water System at Northern China

Changsuo Li [1,2,*], Xingzhou Zhang [1], Xubo Gao [1], Chengcheng Li [1], Chunfang Jiang [1], Wen Liu [2], Guangqi Lin [2], Xin Zhang [1], Jiancong Fang [1], Lijun Ma [1] and Xiubo Zhang [1]

[1] Institute of Geological Survey & School of Environmental Studies, China University of Geosciences, Wuhan 430074, China; xingzhou20220107@163.com (X.Z.); xubo.gao.cug@gmail.com (X.G.); chengcheng009019@hotmail.com (C.L.); cfjcug@163.com (C.J.); ddxnm2022@163.com (X.Z.); fangjiancong1996@163.com (J.F.); mlj-2687@163.com (L.M.); zb2020326@163.com (X.Z.)

[2] 801 Institute of Hydrogeology and Engineering Geology, Shandong Provincial Bureau of Geology & Mineral Resources, Jinan 250014, China; liuwen37801@163.com (W.L.); guangqili@163.com (G.L.)

* Correspondence: lichangsuo20220108@163.com; Tel.: +86-188-0531-8833

Abstract: Karst water quality degradation has been a challenge for domestic and industrial water supplies worldwide. To reveal the possible factors response for karst water quality degradation, Baotu karst spring system is studied as an representative example. In this study, a hydrogeochemical investigation and mathematical, statistical, and geochemical modeling was conducted together to identify the major hydrochemical processes involved in the degradation process. It is found that the karst water is normally fresh, neutral-to-slightly alkaline, with calcium and magnesium as the predominant cations, and bicarbonate and sulfate as the predominant anions. The abnormally high chloride (95.05 mg/L) and nitrate concentrations (148.4 mg/L) give clues to the potential source of contamination in some karst water. The main hydrochemical facies of karst water are HCO_3-Ca and $HCO_3 \times SO_4$-Ca, accounting for 76% of water samples. The water hydrochemistry is controlled mainly by the dissolution of carbonate minerals (calcite, dolomite), followed by the dissolution of silicate and gypsum. The dissolution of calcite and dolomite mostly happens in the recharge area. In the discharge area, the karst water is basically in equilibrium with calcite. The negative SI value of gypsum represents that the water–gypsum interaction is dominated by dissolution along the whole flow path. Cation exchange is observed in the karst water in the indirect recharge area. Along the flow path, the contents of chloride, sulfate, nitrate, and TDS (Total dissolved solids, abbreviated TDS, indicates how many milligrams of dissolved solids are dissolved in one liter of water) vary significantly, which is mostly affected by pollution from human industrial and agricultural activities. The concentrations of major ions were maintained at a low level (<20 mg/L) in the 1960s in karst water. The fast elevation of the parameter values has occurred in the past two decades. The temporal elevation of some pollutants in karst water suggest that global changes (acid rain) and human activity (such as overusing fertilizer) are main factors resulting in the degradation of karst water quality in the study area. The results of this paper provide invaluable information for the management and protection of karst water resources in the urban and rural areas.

Keywords: karst water; karst aquifer minerals; water–rock interaction; groundwater quality; Baotu spring

Citation: Li, C.; Zhang, X.; Gao, X.; Li, C.; Jiang, C.; Liu, W.; Lin, G.; Zhang, X.; Fang, J.; Ma, L.; et al. Spatial and Temporal Evolution of Groundwater Chemistry of Baotu Karst Water System at Northern China. *Minerals* **2022**, *12*, 348. https://doi.org/10.3390/min12030348

Academic Editor: Javier Sánchez-España

Received: 10 January 2022
Accepted: 7 March 2022
Published: 14 March 2022

1. Introduction

Karst groundwater is an important source for domestic and industrial water supply in karst areas, which provide water for about 25% of the global population [1]. In northern China, karst aquifers provide about half of the drinking water supply. Karst water exploitation has increased year by year since the 1950s. With the development of the socio-economy, domestic, agricultural, and industrial water demand imposes a huge burden on the exploitation of karst water.

Karst aquifers are easy to be contaminated due to their thin soil layers, numerous sinkholes, and well-developed joints and fissures. The pollutants can spread quickly and widely within karst water systems via their distinct but interconnected tunnels and fissures [2,3]. Therefore, karst aquifers are of high vulnerability to the input of contaminants. The rapid increase of population, industrial, and agricultural activities and mining also pose a challenge for the protection of karst water from contamination. Karst water pollution was reported in some major cities in China [4,5] and other countries [6,7]. Discharge of municipal wastewater and contaminated urban runoff have caused elevated chloride and ammonium concentrations in karst water [8,9]. Rapid increases of sulfate, nitrogen, and organic pollutants in karst aquifers are reported by cases from mining areas and farmlands [10–15]. Water pollution and quality degradation have reduced the available karst water resources to a great extent worldwide [16].

Karst water degradation has obtained great attention in northern China, especially in Jinan city, one of the famous cities located in a karst area [17]. Numerous research has focused on the recharge sources, water quality, and water cycle of karst springs. Principal component analyses of multivariate statistics were also used to analyze factors affecting the hydrochemical characteristics of groundwater [18,19]. Based on geological structural conditions investigations and trace elements and tracer experiments, the hydraulic conductivity of the northern section of Qianfoshan fracture is determined. The seepage of river water into karst water is tested on the Yufu river.

As a major diagnostic tool in groundwater hydrology, hydrogeochemical data collection, coupled with multidimensional data analysis, has been used to understand specific hydrogeochemical processes [20–23]. Multivariate statistical techniques have been used to reduce the number of variables or cases, while in principle retaining the same information as in the original data. Factor and cluster analyses, among the most widely used multivariate statistical techniques, have been successfully applied to clarify the contributing hydrogeochemical processes controlling groundwater quality, and to identify the pollution sources in groundwater systems [24–26].

In the present study, hydrogeochemical investigation, statistical analysis, and geochemistry modeling were employed together to reveal the natural and anthropic processes' response to the evolution of the karst water quality of Baotu spring at Jinan city.

2. Geology and Hydrogeology Setting

The Baotu karst spring system is located at central Jinan city, western Shandong Province, east China (Figure 1). The study area is high in the south and low in the north. The study area is bounded by the Dongwu and Mashan fractures to the east and west, respectively. The southern boundary is at the foot of Taishan mountain, and the northern boundary is the intrusive rock mass and the Yellow River [27–30]. The study area is a warm and temperate continental climate. The highest annual temperature was 42 °C, and the lowest annual temperature was −17 °C. The annual average precipitation is 501.47 mm.

In the study area, the major stratigraphic sequences include Quaternary strata, Ordovician strata (the Majiagou Group and Sanshanzi Group), Cambrian strata (the Chaomidian Group, Gushan Group, Zhangxia Group, Mantou Group, and Zhushadong Group), and New Archaean Taishan Group (Figure 1). The major karst aquifers are Zhangxia Formation and Fengshan Formation of the upper Cambrian and Ordovician stratum. The carbonate aquifers are composed mainly of limestone, dolomite limestone, gray dolomite, dolomite, and mendacious limestone.

The Baotu karst water system is recharged by precipitation, mainly in the areas with bare layers of carbonate rocks from the mountain in the south [31,32]. Leakage from rivers and the reservoir also contributes a great deal to groundwater recharge. Karst water flow is controlled generally by topography and faults, moving from the south and southeast to the northwest. Limited by the igneous rocks in the north, groundwater flows upward to the ground surface and forms the well-known springs: the Baotu Spring, the Black Tiger Spring, the Pearl Spring, and the Five Dragon Spring. Karst water extraction is another

main form of aquifer discharge. According to the distribution of the surface watershed and recharge strata, the area is divided into three functional zones: indirect recharge area, direct recharge area, and runoff-discharge areas (Figure 1).

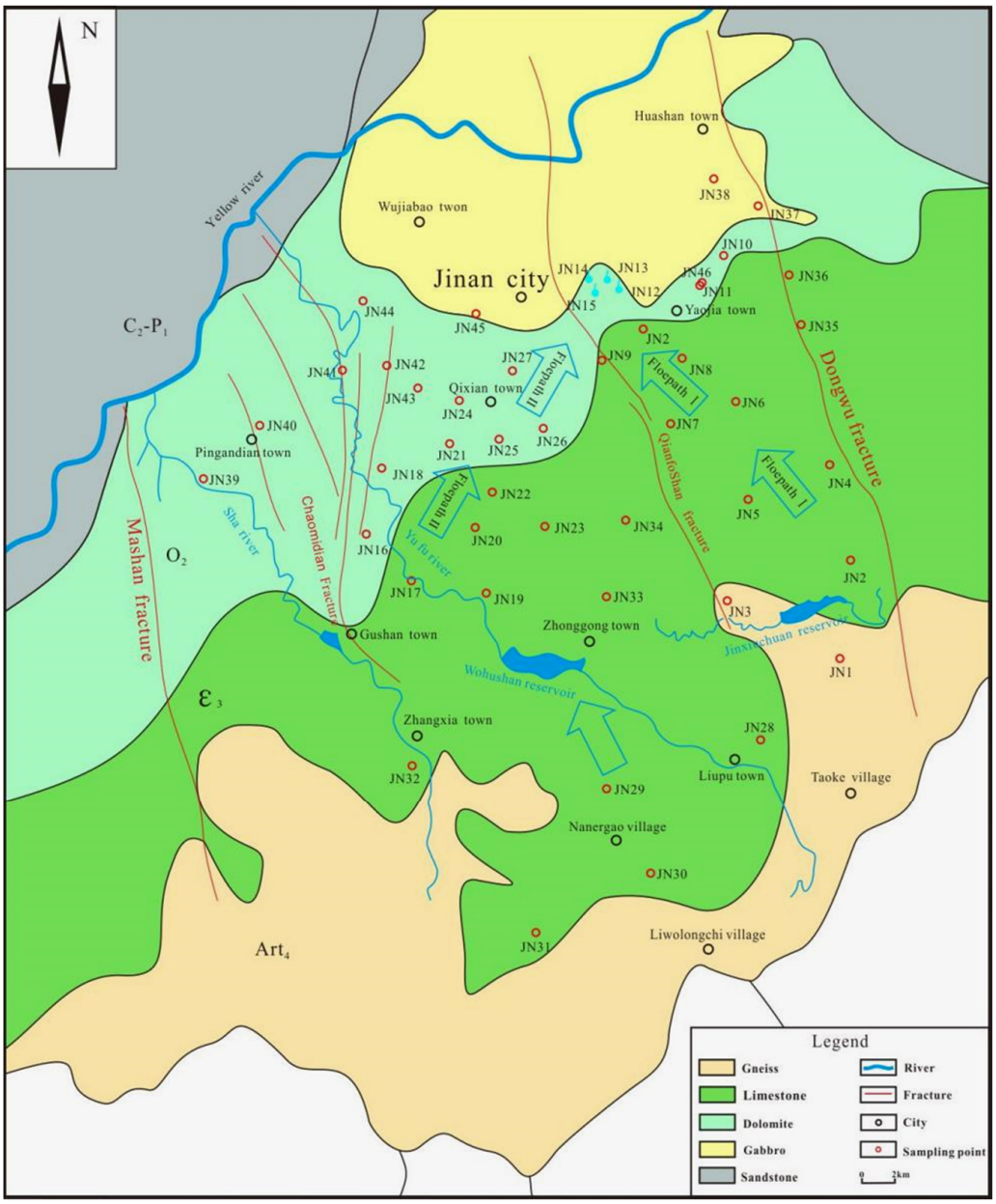

Figure 1. A simple geological map and sampling sites in Baotu karst water system.

3. Sampling and Methods

A total of forty-six karst water samples were collected in October 2020. The general characteristics of the samples are summarized in Table 1.

Table 1. Summary of Chemical data and in situ physico-chemical parameters of the collected karst water samples. Concentration in mg/L, except pH and temperature (T).

	Unit	Min	Max	Average	STD	Variation
pH		7.05	8.06	7.50	0.26	0.03
T	°C	13.70	19.70	16.84	1.46	0.09
DO	mg/l	0.86	10.71	7.34	2.32	0.32
EC	µs/cm	334.00	1324.00	797.12	224.51	0.28
Ca^{2+}	mg/L	10.12	216.20	113.60	39.79	0.35
Mg^{2+}	mg/L	7.43	42.10	19.42	5.86	0.30
Na^{+}	mg/L	3.78	187.47	27.07	27.26	1.01
K^{+}	mg/L	0.38	8.91	1.58	1.33	0.84
HCO_3^{-}	mg/L	80.19	549.86	273.81	70.72	0.26
SO_4^{2-}	mg/L	23.62	187.12	93.38	36.99	0.40
Cl^{-}	mg/L	6.68	95.05	42.16	23.51	0.56
NO_3^{-}	mg/L	1.71	148.44	40.52	34.39	0.85
TDS	mg/L	191.65	822.35	474.63	142.31	0.30

STD, standard deviation.

The locations of the sampling sites, shown in Figure 1, were determined using a portable global positioning system. When sampling, all karst water samples were filtered through 0.45 µm membranes on site and stored with two 550 mL polyethylene bottles. The mutable parameters, such as water temperature, pH, dissolved oxygen and electrical conductivity (EC), were measured in situ using pre-standardized portable Hanna EC and pH meters. Alkalinity was measured on the sampling day using the Gran titration method. Concentrations of anions and cations were determined at the State Key Laboratory of Biological and Environmental Geology, China University of Geosciences (Wuhan), by using ion chromatography (ICS-2100) and ICP-OES (inductive coupled plasma optical emission spectrometer, Puyu Technology), following the US Environmental Protection Agency's standard methods. The estimated analytical errors were within 5%. The mineral saturation index was calculated using the hydrochemical simulation software PHREEQC Interactive 2.17.4137. The historical data (1958–2019) used in this study were collected from the 801 Hydrogeology and engineering Geology Team, the Bureau of Geology and Mineral Exploration of Shandong Province.

4. Results and Discussion

4.1. Karst Water Hydrogeochemistry

The statistical analysis of the forty-six karst water samples are shown in Table 2. The groundwater is normally fresh (TDS 191.7–822.4 mg/L), neutral-to-slightly alkaline (pH 7.00 and 8.06), with temperatures between 13.7 and 19.7 °C. Calcium and magnesium are the predominant cations in the karst water, with concentrations varying from 10.1–216.2 mg/L and 7.43–42.10 mg/L, respectively. The high content of sodium (up to 187.5 mg/L) in some karst water reflects the involvement of cation exchange in groundwater chemistry. The predominant anions are characterized as bicarbonate (80.19–549.9 mg/L) and sulfate (23.62–187.1 mg/L) in the studied karst water and might be attributed to the weathering of carbonate- and sulfate-bearing bedrock. The abnormally high chloride (6.68–95.05 mg/L) and nitrate concentrations (1.71–148.4 mg/L) give clues to the potential contamination of human activities in some karst water.

Table 2. Summary of chemical data and in situ physico-chemical parameters of the collected karst water samples. Concentration in mg/L, except pH and temperature (T).

	Unit	Min	Max	Average	STD	Variation
pH		7.05	8.06	7.50	0.26	0.03
T	°C	13.70	19.70	16.84	1.46	0.09
DO	mg/l	0.86	10.71	7.34	2.32	0.32
EC	µs/cm	334.00	1324.00	797.12	224.51	0.28
Ca^{2+}	mg/L	10.12	216.20	113.60	39.79	0.35
Mg^{2+}	mg/L	7.43	42.10	19.42	5.86	0.30
Na^{+}	mg/L	3.78	187.47	27.07	27.26	1.01
K^{+}	mg/L	0.38	8.91	1.58	1.33	0.84
HCO_3^{-}	mg/L	80.19	549.86	273.81	70.72	0.26
SO_4^{2-}	mg/L	23.62	187.12	93.38	36.99	0.40
Cl^{-}	mg/L	6.68	95.05	42.16	23.51	0.56
NO_3^{-}	mg/L	1.71	148.44	40.52	34.39	0.85
TDS	mg/L	191.65	822.35	474.63	142.31	0.30

STD, standard deviation.

The main hydrochemical type of karst water in the study area was HCO_3-Ca and HCO_3 × SO_4-Ca water (Figure 2a), accounting for 76% of water samples. Meanwhile HCO_3-Ca × Mg-type water represents 13% of the karst water samples. The karst water of the southern indirect recharge area mostly belongs to HCO_3-Ca × Mg-type water. In direct recharge areas, karst water is HCO_3 × SO_4-Ca-type water. In the runoff areas and discharge areas, karst water and spring water normally belong to HCO_3-Ca-type water, except for the Baotu Spring and Black Tiger Spring. The significant differences in the water chemical types indicate the diversity of flow path and cycle model of karst springs in the area. When salinity is considered, the karst water samples are plotted as total salinity (TIS) (Figure 2b). The TIS of karst water in the indirect recharge area and runoff-discharge area is mostly concentrated in 8–16 meq/L, and the TIS of karst water in the direct recharge area is concentrated in 12–20 meq/L; the TIS of karst water in the direct recharge area is higher than that of karst water in the indirect recharge area and runoff-discharge area.

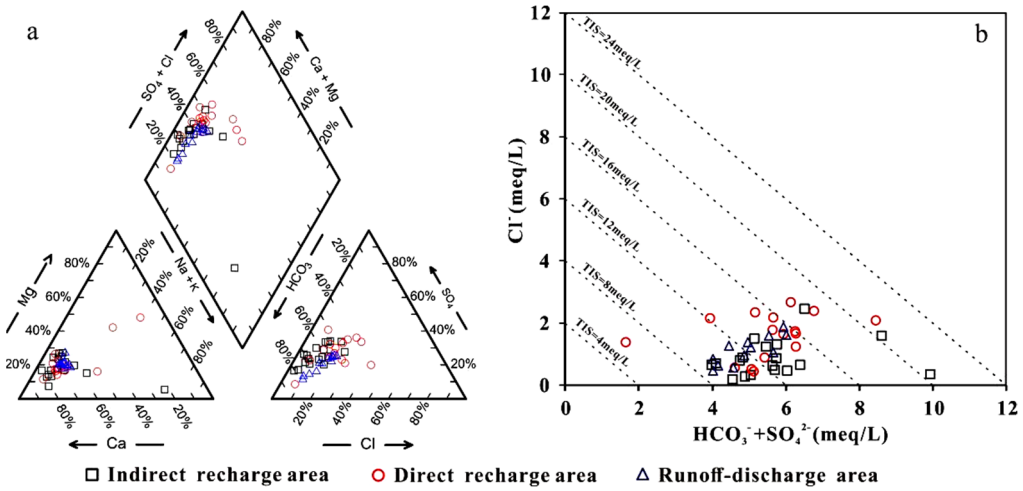

Figure 2. Piper diagram (**a**) and TIS diagram (**b**) of karst water from the Baotu Karst Spring system.

4.2. Karst Water–Aquifer Interaction

4.2.1. Potential Sources of Groundwater Components

The Gibbs plots has been widely used to distinguish between the three mechanisms that affect groundwater components: rock weathering, evaporation–concentration, and atmospheric precipitation [33]. As shown in Figure 3, most of the karst water samples fall into the rock weathering area, with the TDS between 190–830 mg/L and

$Cl^-/(Cl^- + HCO_3^-)$ ratio <0.4. This indicates that weathering dissolution of aquifer minerals is the most important process controlling groundwater hydrogeochemistry in the Baotu karst spring area. However, some of the karst water samples from the direct and indirect recharge areas fell within region II, with a higher $Na^+/(Na^+ + Ca^{2+})$ value. Due to the low abundance of sodium in the karst aquifer media, it is preliminary recommended that karst water chemistry may be affected by cation exchange or the pollution of anthropic activities.

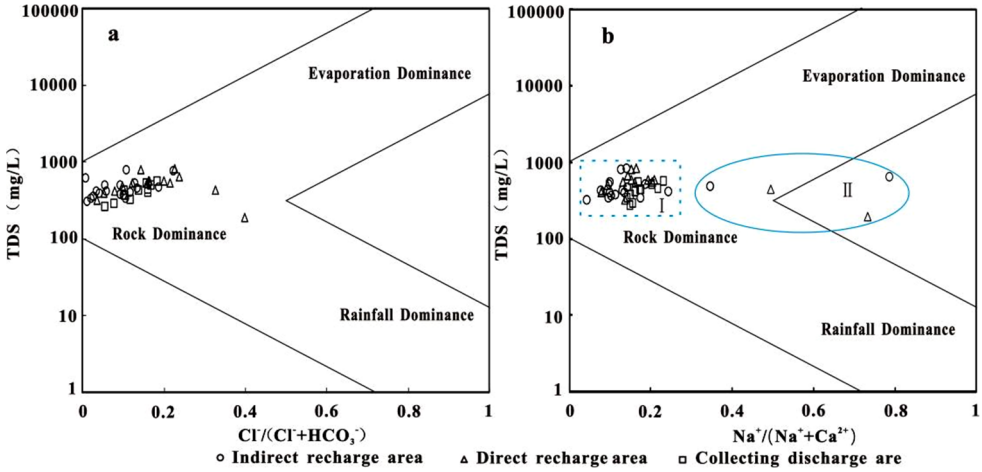

Figure 3. Gibbs diagram of karst water samples in the Baotu karst spring system ((**a**) $Cl^-/(Cl^- + HCO^{3-})$ and (**b**) Na+/$(Na^+ + Ca^{2+})$.

As shown in Figure 4, most of the karst samples are concentrated between the silicate and carbonate end members, indicating that the ionic components in the karst water come mainly from the weathering dissolution of carbonates and silicates. According to the distribution pattern of karst water samples in Figure 4, it is obvious that most of the karst water is distributed mainly near the carbonate end member. Meanwhile, they all have a higher HCO_3/Na and Ca/Na ratio and a moderate-to-low Mg/Na ratio. Therefore, we moderately concluded that the supply source of the main ions is the weathering dissolution of carbonates, especially calcite. Some of the karst water in zone I, mainly from recharge areas, is distributed near the silicate end member, suggesting that it may be recharged by fissure water, pore water, surface water, or even contaminated water.

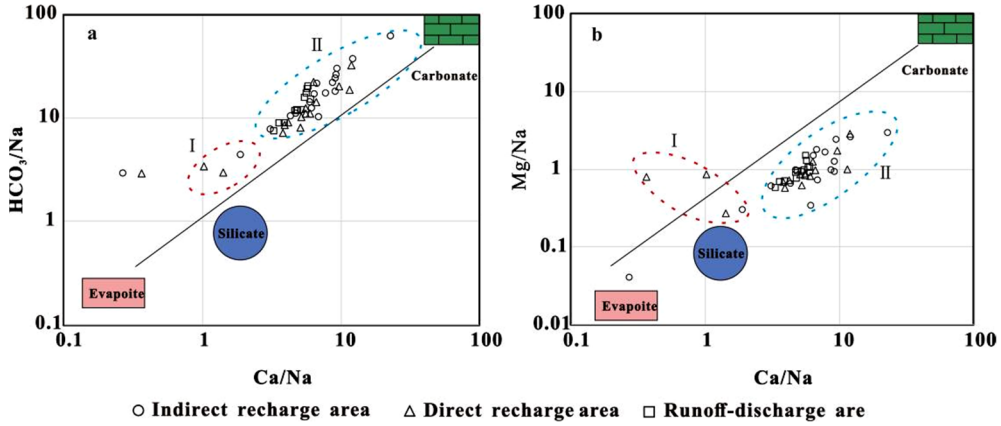

Figure 4. Ion ratio scatter map of karst water in the Baotu karst spring system ((**a**) HCO_3/Na and (**b**) Mg/Na).

4.2.2. The Dissolution of Major Minerals

The mineral dissolution equations for carbonate, silicate, and evaporite in the karst aquifer are as follows:

$$CaCO_3 + CO_2 + H_2O = Ca^{2+} + 2HCO_{3\_} \quad (1)$$

$$CaSO_4 + 2H_2O = Ca^{2+} + SO_4{}^{2-} + 2H_2O \quad (2)$$

$$CaMg(HCO_3)_2 + 2CO_2 + 2H_2O = Ca^{2+} + Mg^{2+} + 4HCO_3 \quad (3)$$

$$\text{Silicate} + H_2CO_3 = H_4SiO_4 + HCO_3{}^- + Na^+ + K^+ + Mg^{2+} + Ca^{2+} + \text{kaolinite} \quad (4)$$

(Na, Mg, Ca, K)

Based on the dissolution equations, the groundwater ion ratios are used to reveal the major geochemical mechanisms that control the overall geochemical composition of karst water [34]. For example, the $(Ca^{2+} + Mg^{2+})/(HCO_3{}^- + SO_4{}^{2-})$ ratio is used to determine the dissolution status of carbonate and silicate. The $(Ca^{2+} - HCO_3{}^-)/SO_4{}^{2-}$ ratio is employed to explain a non-carbonate Ca^{2+} from the dissolution of gypsum. The Ca^{2+}/Mg^{2+} ratio is used to indicate the dissolution contribution of calcite and dolomite in the carbonate system, and a ratio of Na^+/Cl^- is used as an indicator of halite (NaCl) dissolution.

Carbonate Dissolution

A $Ca^{2+} + Mg^{2+}$ versus $HCO_3{}^- + SO_4{}^{2-}$ scatter map is used to identify the dissolution of carbonate (Figure 5a). Most of the sampling sites are located near and above the 1:1 line, indicating that the main ions in karst water come from the dissolution of carbonate rock and gypsum, and the dissolution of karst aquifers is the main process of karst water chemistry. Part of the karst water samples from the direct and indirect recharge area is far away from the 1:1 line, which may be affected by human activity and or surface-water infiltration [35,36].

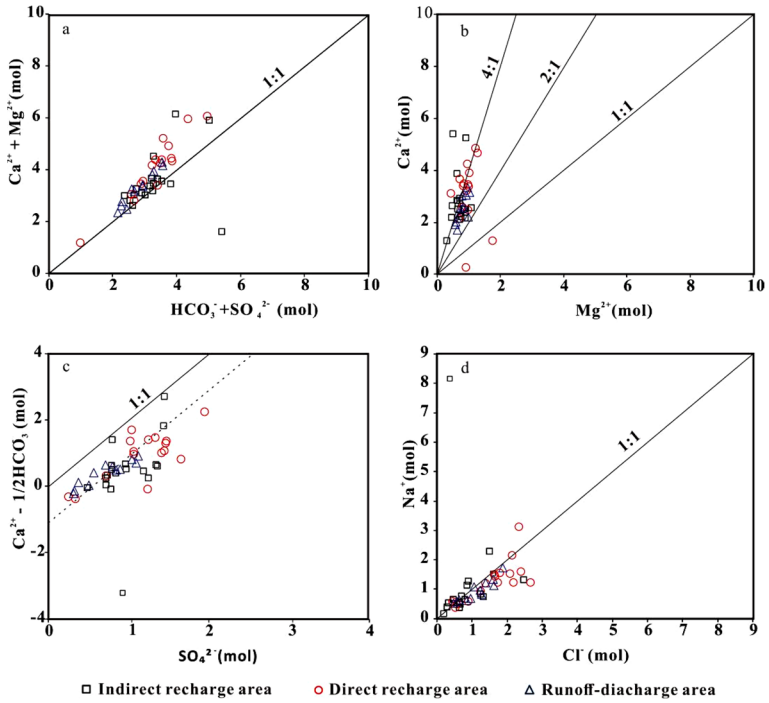

Figure 5. Ion ratio scatter map of karst water in Baotu karst spring system ((**a**) $(Ca^{2+} + Mg^{2+})$ vs. $(SO_4{}^{2-} + HCO_3)$; (**b**) Ca^{2+} vs. Mg^{2+}; (**c**) $Ca^{2+} - 1/2HCO_3{}^-$ vs. $SO_4{}^{2-}$; (**d**) Na^+ vs. Cl^-).

A Ca^{2+} VS Mg^{2+} scatter plot may provide invaluable information on the dissolution of calcite or dolomite in karst water (Figure 5b). Most karst water samples fall above the

straight 2:1 line, around the 4:1 line, which illustrated that calcium in karst water comes mainly from the dissolution of calcite, and that a small part comes from the dissolution of dolomite and gypsum. Meanwhile, two karst water samples, from the direct recharge area, are located below the 1:1 line, which may be the contribution of dolomite dissolution or the cation alternation adsorption [37,38].

Evaporite Dissolution

As seen from Figure 5c, karst water samples are distributed mainly below the 1:1 line of $Ca^{2+} - 1/2HCO_3^-$: SO_4^{2-} and near the parallel line (near the dotted line). $Ca^{2+} - 1/2HCO_3^-$ increases with the increase of SO_4^{2+} content, indicating that the dissolution of gypsum is also one of the hydrochemical processes of karst water, and also indicates that there are other sources of Ca^{2+} in karst water. According to Figure 5d, most of the karst water is distributed on and near the 1:1 line of Cl^-: Na^+, which means the Na^+ and Cl^- comes mainly from the dissolution of halite. The samples that are far from the 1:1 line may suffer from the contamination of domestic wastewater.

4.2.3. Cation Exchange

A Scatter plot of (Ca + Mg) − (SO_4 + HCO_3) vs. (Na + K − Cl) is used to determine whether cation exchange occurs in karst water. A Na+ K − Cl value represents the non-halite-sourcing sodium, while (Ca + Mg) − (SO_4 + HCO_3) represents the sum of Ca^{2+} and Mg^{2+} in groundwater, except for carbonate and sulfate dissolution sources. An elevation of the $Na^+ + K^+ - Cl^-$ value and a decrease of the $Ca^{2+} + Mg^{2+}$ value or an increase of the $SO_4^{2-} + HCO_3^-$ value may indicate the occurrence of cation exchange in groundwater. Additionally, if the two have a linear relationship and the slope is −1, the ion exchange is significant in groundwater. As can be known from Figure 6, the fitting line of the karst water from the indirect recharge area is y = −1.1304x + 0.7721, and the fitting line of the karst water from the runoff-discharge area is y = −1.3046x + 0.7369. Obviously, cation exchange is one of the major processes that control the formation of karst water chemistry in the indirect recharge areas and the runoff-discharge areas, but not in the direct recharge areas.

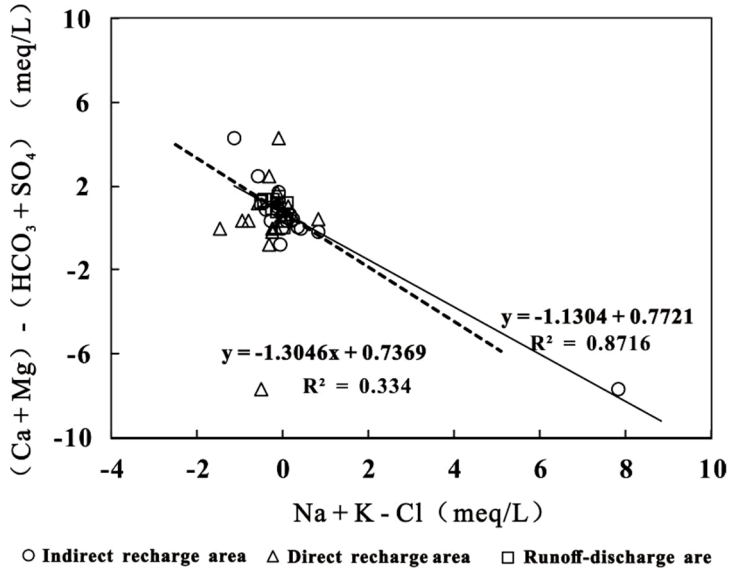

Figure 6. (Ca + Mg) − (HCO_3 + SO_4) vs. Na + K − Cl scatter plot of karst water from the Baotu karst spring system.

4.3. The Spatial and Temporal Variation of Karst Water Chemistry

4.3.1. Variation of Karst Water Chemistry along the Flow Path

Major Ions

The chemical evolution of karst water was investigated along two main flow paths: (1) Flow Path I (the south–north flow path), from the south recharge area to the discharge area; (2) Flow Path II (the west–north flow path), from the leakage area (Yufu river) to the discharge area.

In Figure 7, the anions and TDS content showed an overall increasing trend in Flow Path I. In the indirect recharge area, the content of SO_4^{2-} and NO_3^- is high in karst water sample JN3, showing that the karst water there is strongly contaminated by agricultural activity. This also reflects that, in the indirect recharge area, groundwater is stored mainly in shallow fissured aquifers, with a small buried depth, which puts groundwater at a high risk of contamination by industrial, agricultural, and other human activities.

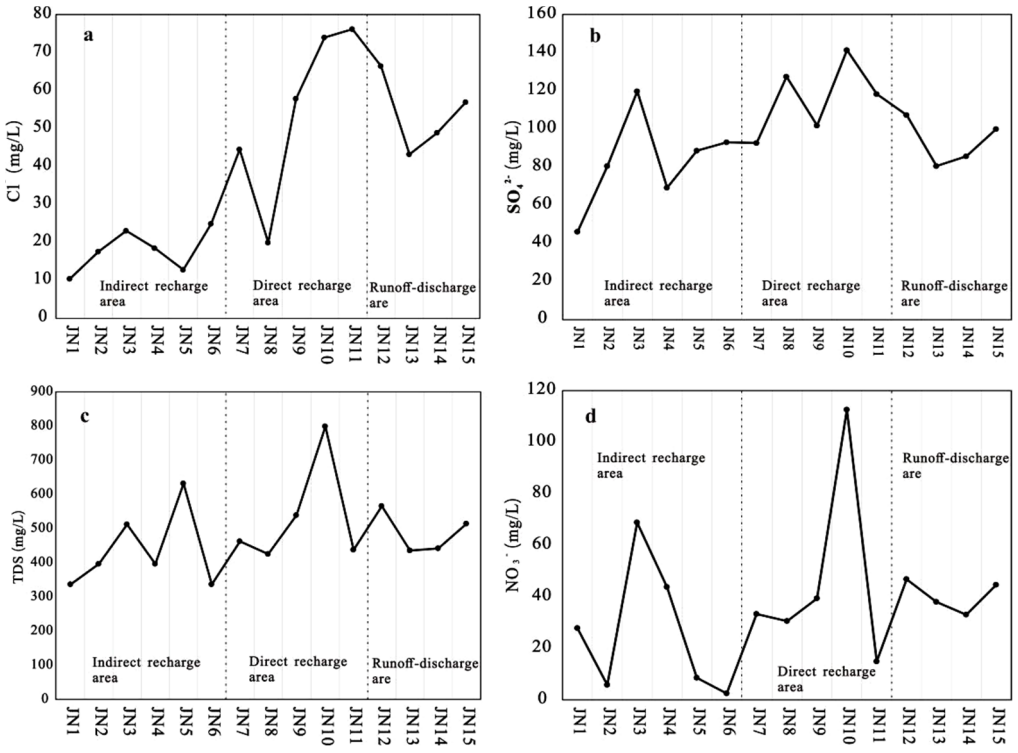

Figure 7. Variation of ion components ((**a**) Cl^-; (**b**) SO_4^{2-}; (**c**) TDS; (**d**) NO_3^-) in karst water along Flow Path I (south → north).

The karst water with the highest anion content, especially the Cl^- and NO_3^-, is derived mainly from the direct recharge area. The highest Cl^- concentration was observed in karst water sample JN11, and the highest content of NO_3^- was found in karst water JN10. Due to the low background concentrations of both Cl^- and NO_3^- in karst aquifers, the extremely high Cl^- and NO_3^- content represents the direct pollution threat of karst water from agricultural activity, non-point source pollution, and domestic sewage wastewater discharge. An elevation of SO_4^{2-} concentration occurs in almost all of the karst water samples. A field investigation suggested that there is no non-point source pollution in the study area. Thus, the most possible source of sulfates may come from the weathering dissolution of gypsum in the carbonates. Under the influence of climate change and human activity, the water–rock interaction is intensified in the epikarst. The deceased ion content of karst water in the discharge area may be due to the recharge of local water with low TDS and ion concentrations.

As shown in Figure 8, the contents of chloride, sulfate, nitrate, and TDS vary significantly along Flow Path II. In the indirect recharge area, their values in some karst water samples are higher than most of the karst water in the area, because some reaches of Yufu River have water infiltration and recharge groundwater. Therefore, it is inferred that the high ion concentration in these karst water is coming from the leakage contamination of surface water, especially the river water and runoff water. Due to the weak protection ability of karst water in the leakage areas, polluted surface water and dirty wastewater, generated by industrial and agricultural activities, can easily enter the karst aquifers through the leakage section, causing karst water pollution.

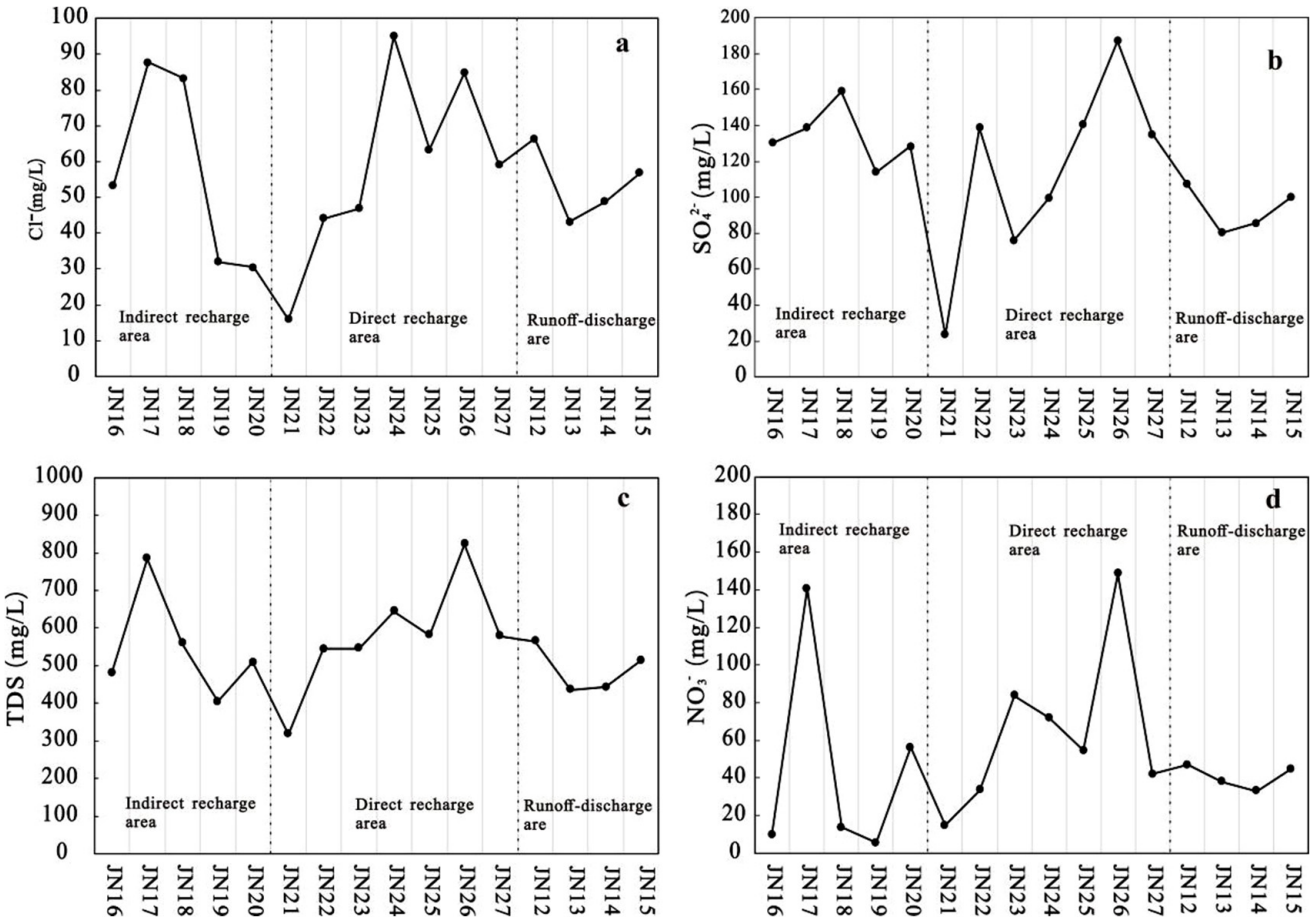

Figure 8. Variation of ion components ((**a**) Cl^-; (**b**) $SO_4{}^{2-}$; (**c**) TDS; (**d**) $NO_3{}^-$) in karst water along Flow Path II (west → north).

In the direct recharge area, karst water with the highest content of Cl^- and $NO_3{}^-$ was observed. The high content of Cl^- (>50 mg/L) in karst water means that a common phenomenon of domestic sewage leakage and karst water pollution occurs in the area. At the same time, there is also a local karst water pollution caused by the use of chemical fertilizers in agricultural activities, indicated from the high content of nitrate (>40 mg/L) in some karst water.

Minerals Saturation Index

The mineral saturation index of karst water, as shown in Table 3, was calculated by using PHREEQC Interactive 2.17.4137 (PHREEQC is a computer software used to calculate a variety of cryogenic hydrogeochemical reactions.). Along Flow Path I, the value of $SI_{calcite}$ (saturation index of calcite) ranges from −0.02 to 0.88 (Table 3). In the indirect recharge area, the $SI_{calcite}$ value of most karst water is less than 0.5, which indicates a dissolution of

calcite in the karst water system. In the direct recharge area, the $SI_{calcite}$ value increased and the karst water reached an over-saturation state of calcite. In the discharge area, the $SI_{calcite}$ value is stable at about 0.5, indicating that karst water is, basically, in equilibrium with calcite.

Table 3. Mineral saturation index table of karst water sampling points on runoff path.

Number	Calcite	Dolomite	Gypsum	Number	Calcite	Dolomite	Gypsum
JN1	−0.01	−0.41	−1.62	JN16	0.41	0.36	−1.42
JN1	0.44	0.62	−1.9	JN17	0.78	0.93	−1.22
JN2	0.59	0.65	−1.56	JN18	0.37	0.36	−1.35
JN3	0.58	0.63	−1.43	JN19	0.37	0.37	−1.49
JN4	0.48	0.68	−1.69	JN20	0.52	0.55	−1.4
JN5	0.47	0.45	−1.88	JN21	0.49	0.62	−2.17
JN6	0.28	0.22	−1.59	JN22	0.63	0.77	−1.3
JN7	0.55	0.62	−1.51	JN23	0.69	0.73	−1.52
JN8	0.44	0.16	−1.34	JN24	0.73	0.94	−1.4
JN9	0.63	0.78	−1.44	JN25	0.55	0.7	−1.32
JN10	0.88	1.29	−1.25	JN26	0.7	0.97	−1.14
JN11	−0.02	0.23	−1.75	JN27	0.63	0.83	−1.33
JN12	0.61	0.81	−1.44	JN14	0.61	0.81	−1.44
JN13	0.48	0.59	−1.61	JN13	0.48	0.59	−1.61
JN14	0.46	0.54	−1.59	JN14	0.46	0.54	−1.59
JN15	0.56	0.71	−1.48	JN15	0.56	0.71	−1.48

Along Flow Path I (Figure 9a), the saturation index of dolomite ($SI_{dolomite}$) ranged from 0.16 to 1.29 (with a mean value of 0.59). In the indirect recharge area, $SI_{dolomite}$ was mostly larger than 0.5, indicating that karst water is over-saturated to dolomite. In the direct recharge area, the $SI_{dolomite}$ in karst water further increased, especially in the sample from JN10, where the $SI_{dolomite}$ was 1.29, showing a significant precipitation status. However, a lower $SI_{calcite}$ (−0.02) and $SI_{dolomite}$ (0.16) index was found in karst water (JN11) from the direct recharge area. Considering the higher Cl^- concentration and ^2H and ^{18}O isotopic values, it can be judged that the karst water is seriously affected by the leak recharge of surface water.

Along Flow Path I, the saturation index of gypsum (SI_{gypsum}) ranged from −1.9 to −1.25, with a mean value of −1.56. It can be seen that karst water is always able to dissolve gypsum during the movement in the aquifers.

In Flow Path II (Figure 9b), the $SI_{calcite}$ and $SI_{dolomite}$ values of karst water was 0.37–0.78 and 0.36–0.97, respectively, with a mean value of 0.56 and 0.67. A slight increase of the $SI_{calcite}$ and $SI_{dolomite}$ value was observed along the flow path. In the indirect recharge area, both saturation indexes of calcite and dolomite were below 0.5 (except for sample JN17), indicating that the weathering dissolution was mainly water–rock interaction processes between karst water and aquifer minerals (calcite and dolomite). When the karst water moved into the direct recharge area, the mineral saturation index gradually increased up to 0.5, demonstrating that the interaction of karst water and aquifer minerals is dominated by dissolution–precipitation. A decline of the mineral saturation index in karst water in the discharge area represents the transformation of water–rock interaction modes, due to the reception of a large sum of local water source recharge.

Along Flow Path II, the saturation index of gypsum changes from −2.17 to −1.14, with a mean of −1.44. The negative SI_{gypsm} value in karst water represents that the water–gypsum interaction is dominated by dissolution during the movement.

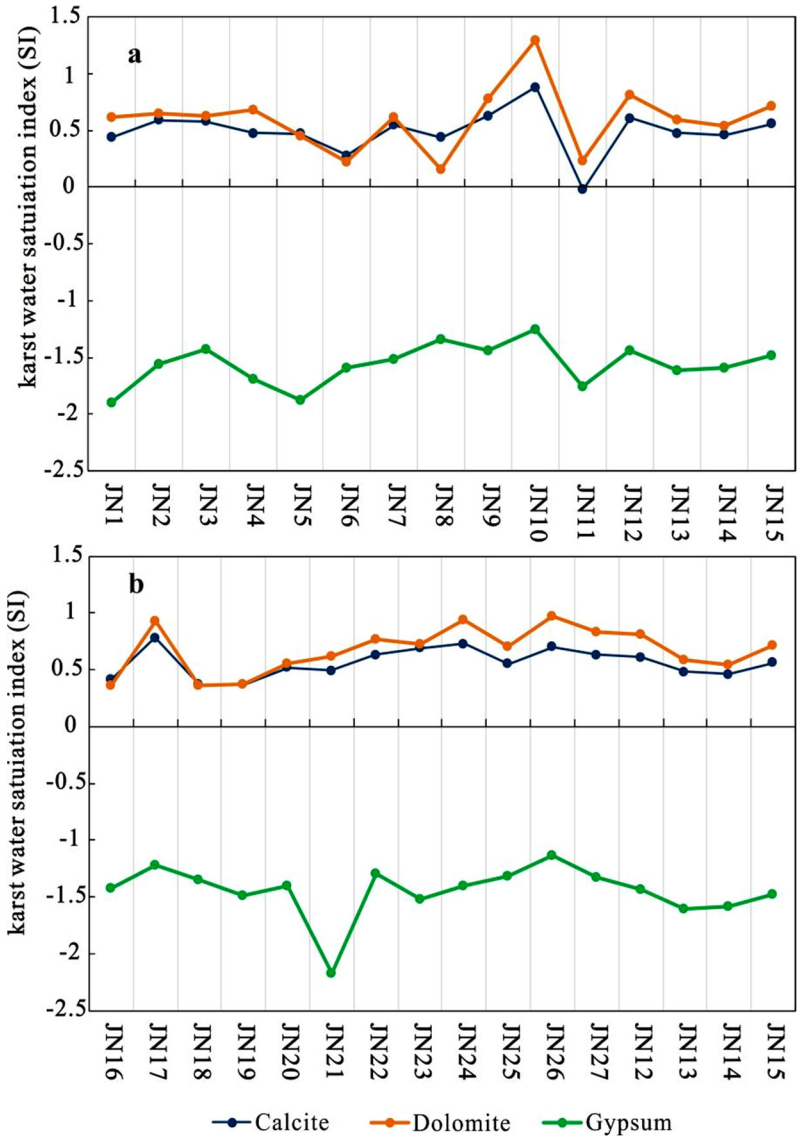

Figure 9. The mineral saturation index of calcite, dolomite, and gypsum in the karst aquifers along Flow Paths I and II. (**a**) Flow Path I (the south–north flow path), from the south recharge area to the discharge area; (**b**) Flow Path II (the west–north flow path), from the leakage area (Yufu river) to the discharge area.

4.3.2. Temporal Evolution of Karst Water Hydrochemistry

The monitoring data of main chemical parameters (K + Na, Ca, Mg, HCO_3, SO_4, Cl, NO_3, Total hardness, TDS) of Baotu Spring are shown in Figure 10. The concentrations of major ions were maintained at a low level (<20 mg/L) in the 1960s. A slight elevation of the value of the parameters was found after that. The significant increases of the parameter values happened in the 1980s. A fast elevation of the parameter values occurred in the past two decades. Right now, The content of SO_4^{2-}, Cl^-, NO_3^-, Ca^{2+}, and TDS are up to 100 mg/L, 50 mg/L, 40 mg/L, 120 mg/L, and 600 mg/L, respectively. Part of the values are higher than both the max limitation value for drinking water in China and the recommendation value of the EPA.

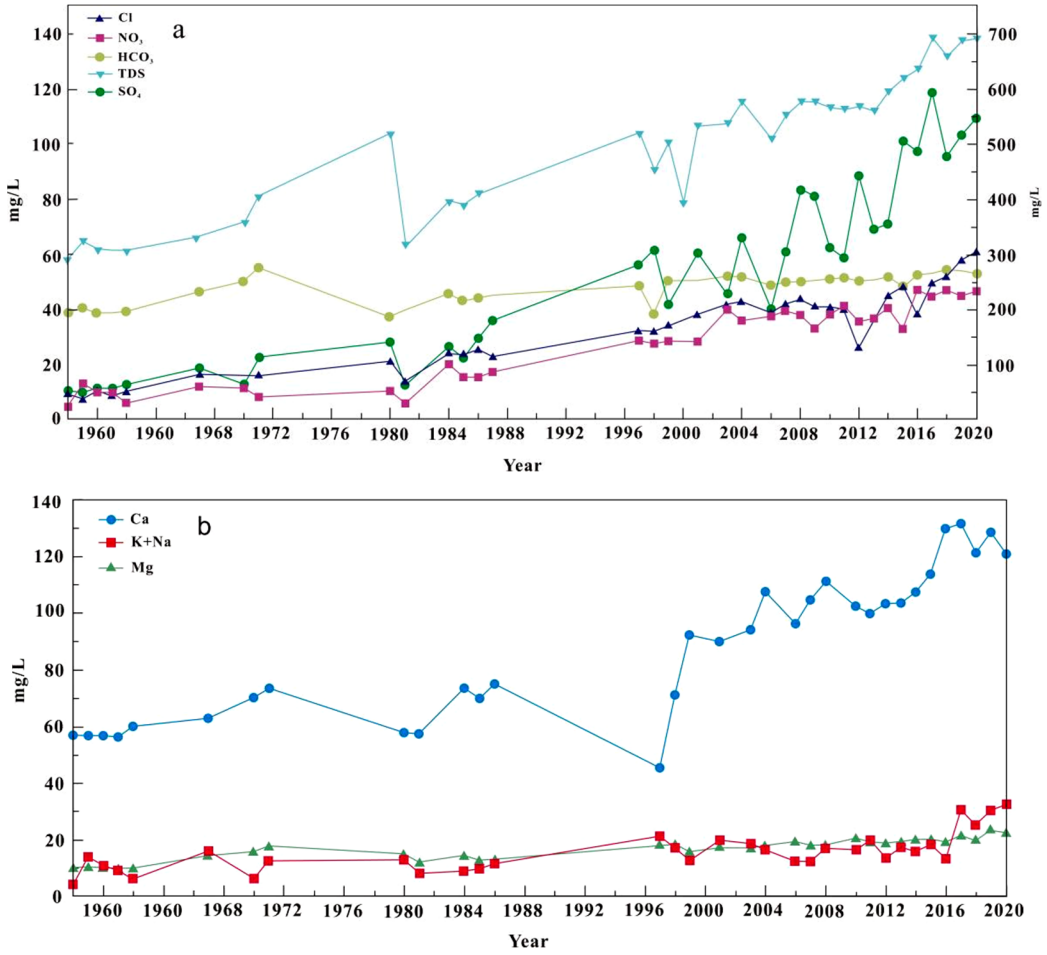

Figure 10. Variation of major ions ((**a**) TDS, Cl, NO_3, HCO_3, SO_4; (**b**) Ca, K+Na, Mg) in Baotu Spring water from 1958–2020. TDS and HCO3 look at the right axis.

The elevation of TDS, sulfate, nitrate, and chloride concentrations in karst water were illustrated in Figure 11. It is noticed that the average elevation of TDS is more than 200 mg/L, with the highest value reaching more than 700 mg/L. Meanwhile, the highest increase of sulfate, nitrate, and chloride concentrations are more than 200 mg/L, 50 mg/L, and 30 mg/L, respectively.

The spatial discrepancy of ion concentrations reflects the pollution caused the elevation of ions in karst water. Due to the lack of nitrogen-containing minerals in the karst strata in the study area, the higher nitrate concentrations in the karst water were derived mainly from the effects of human activity, especially agricultural activities.

The dissolution of evaporates (halite) is one of the main sources of chloride in karst water. However, the rapid increase of chloride concentration in karst water is not accompanied by a coincident increase of sodium content. It can be deduced that the higher chloride concentration in the karst water is not the result of the dissolution of the evaporates, such as halite. Therefore, it can be concluded that a high chloride content in karst water should be the result of domestic sewage discharge or surface-water leakage pollution.

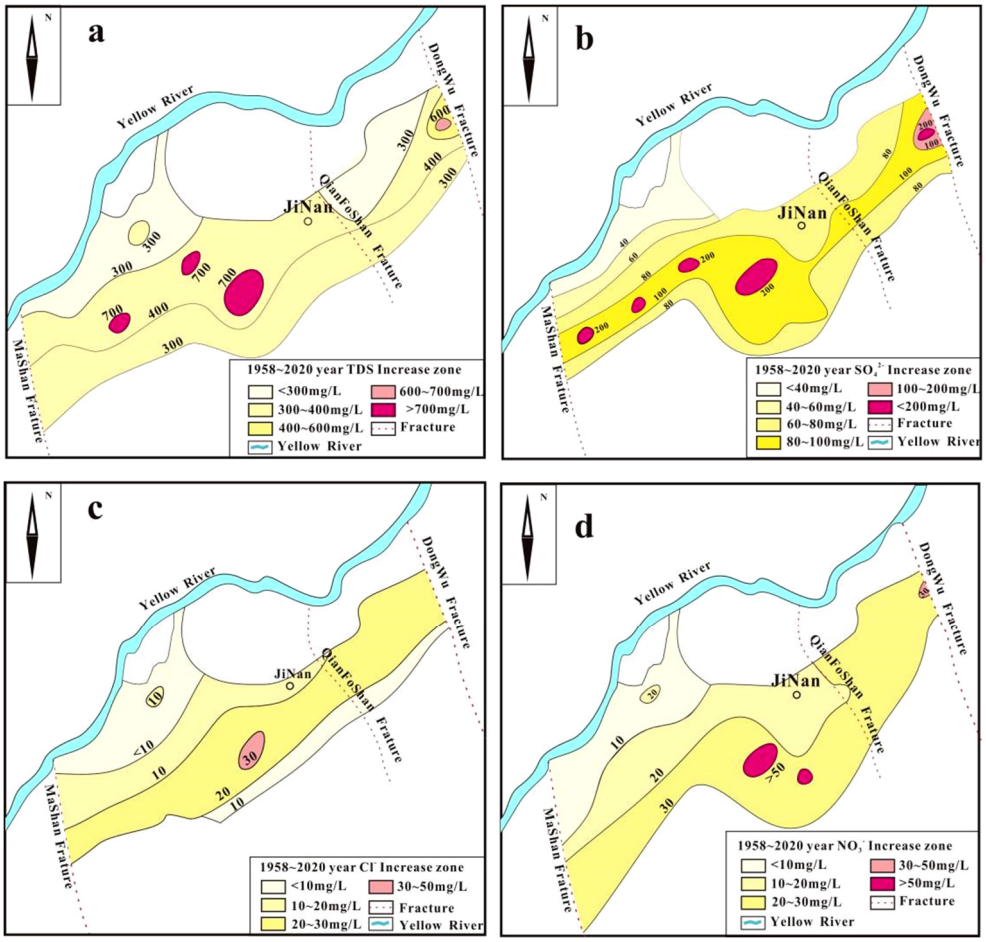

Figure 11. Elevation of major parameters ((**a**) TDS; (**b**) SO_4^{2-}; (**c**) Cl^-, (**d**) NO_3^-) in karst water during 1958–2020.

The sulfate concentration was also significantly increased in the karst water and spring water (from 5 mg/L to nearly 100 mg/L). According to our field investigation, there is no sulfate-related industry or mines, so industrial and mining activity are not the reason for the elevation of sulfate in karst water in the study area. The large-scale increase of sulfate in karst water may be related to the local acid rain and the acidic weathering dissolution of gypsum. With the rapid development of social economy, increased demand for energy, such as coal mining and combustion cause a high content of sulfur in the rainfall. Therefore, precipitation may bring more sulfate into surface water and also on groundwater (pore water, fissure water, and karst water). Moreover, the acid rain falls to the ground, reacts with the exposed carbonate formation, promotes the weathering dissolution of sulfate-bearing minerals (e.g., gypsum) in the karst formation, and brings more sulfate into the karst water.

Agricultural activity (such as using fertilizer), as another factor, may also be responsible for the large-scale increase of sulfate and nitrate in karst water. In the south indirect recharge area, the land (base rock) is covered by a thin layer of weathered soil. Agriculture activity is popular in the area. Overusing sulfate and nitrate fertilizers is common to improve the production of crops. The large amount of fertilizer brings sulfate and nitrate into rivers and groundwater by surface infiltration.

5. Conclusions

The karst water from the Baotu karst spring system is normally fresh, neutral-to-slightly alkaline, with calcium, magnesium, bicarbonate, and sulfate as the predominant cations and anions. An abnormally higher chloride (6.68–95.05 mg/L) and nitrate concen-

tration (1.71–148.4 mg/L) was found in some karst water, which gives clues to the potential source of contamination.

The main hydrochemical type of karst water was HCO_3-Ca and $HCO_3 \times SO_4$-Ca, accounting for 76% of water samples. Meanwhile, HCO_3-Ca × Mg-type water represented 13% of the karst water samples. The water hydrochemistry is controlled mainly by the dissolution of carbonate minerals (calcite, dolomite), followed by the dissolution of silicate and gypsum. The cation exchange is obvious in the karst water in the indirect recharge area, but not in the direct recharge area.

Along the karst water flow path, the contents of chloride, sulfate, nitrate, and TDS vary significantly, which is mostly affected by pollution from human industrial and agricultural activities. The dissolution of calcite and dolomite mostly happens in the recharge area. In the discharge area, the karst water is, basically, in equilibrium with calcite. The negative SI value of gypsum represents that the water–gypsum interaction is dominated by dissolution along the whole flow path.

The concentrations of major ions were maintained at a low level (<20 mg/L) in the 1960s in karst water. The fast elevation of the parameter values occurred in the past two decades. Right now, some of the values are higher than the max limitation value for drinking water in China, and also than the recommended value of the EPA. The temporal elevation of some pollutants in karst water suggest that global changes (acid rain) and human activity (such as overusing fertilizer) are main factors resulting in the degradation of karst water quality in the study area.

Author Contributions: Conceptualization, C.L. (Changsuo Li) and X.Z. (Xingzhou Zhang); Data curation, X.Z. (Xingzhou Zhang), G.L., L.M. and X.Z. (Xiubo Zhang); Funding acquisition, X.Z. (Xingzhou Zhang); Investigation, X.Z. (Xingzhou Zhang), C.J., W.L. and J.F.; Methodology, X.Z. (Xingzhou Zhang); Project administration, X.G.; Software, C.L. (Chengcheng Li); Validation, X.Z. (Xin Zhang); Writing–original draft, X.Z. (Xingzhou Zhang); Writing–review & editing, X.Z. (Xingzhou Zhang) and X.G. All authors have read and agreed to the published version of the manuscript.

Funding: This research was financially supported by the National Natural Science Foundation of China (nos. 42172288, 41902265 and 41877204), the 111 Program (State Administration of Foreign Experts Affairs and the Ministry of Education of China, B18049), Guangxi Key Science and Technology Innovation Base on Karst Dynamics (KDL&Guangxi202001), and the open funding of Shandong Engineering Research Center for Environmental Protection and Remediation on Groundwater.

Data Availability Statement: The data used to support the findings of this study are included within the article.

Acknowledgments: We would like to thank 801 Institute of Hydrogeology and Engineering Geology, Shandong Provincial Bureau of Geology for providing background information on the study area. We thank Shuai Gao, Xing Cheng, Hongyu Li, Pei Li Gong, Zhendong Pan, Shiqi Li and Duan Yan for their assistance in the field and laboratory work.

Conflicts of Interest: The authors declare no conflict of interest.

References

1. Ford, D.; Williams, P. *Karst Hydrogeology and Geomorphology*; John Wiley and Sons: Chichester, UK, 2007.
2. Sanchez, D.; Barbera, J.A.; Mudarra, M.; Andreo, B. Hydrogeochemical tools applied to the study of carbonate aquifers: Examples from some karst systems of Southern Spain. *Environ. Earth Sci.* **2015**, *74*, 199–215. [CrossRef]
3. Bonacci, O.; Pipan, T.; Culver, D.C. Karst ecohydrological framework. *Environ. Geol.* **2009**, *56*, 891–900. [CrossRef]
4. Kurniawan, I.A.; Adji, T.N.; Nurkholis, A.; Haryono, E.; Fatoni, H.; Waskito, W.A.; Cahyadi, A.; Agniy, R.F. Karst aquifer response by time series analysis applications in Jonggrangan Karst, Java Island, Indonesia. *Environ. Earth Sci.* **2019**, *78*, 379. [CrossRef]
5. Wu, X.; Gao, X.; Tan, T.; Li, C.; Yan, R.; Chi, Z.; Feng, Y.; Gong, P.; Fang, J.; Zhang, X.; et al. Sources and pollution path identification of PAHs in karst aquifers: An example from Liulin karst water system, northern China. *J. Contam. Hydrol.* **2021**, *241*, 103810. [CrossRef]
6. Goldscheider, N.; Chen, Z.; Auler, A.S.; Bakalowicz, M.; Broda, S.; Drew, D.; Hartmann, J.; Jiang, G.; Moosdorf, N.; Stevanovic, Z.; et al. Global carbonate distribution and karst water resources. *Chin. J. Hydrogeol.* **2020**, *28*, 1661–1677. [CrossRef]
7. Drew, D.; Hötzl, H. Karst Hydrogeology and Human Activities: Impacts, Consequences, and Implications. *Environ. Eng. Geosci.* **1999**, *4*, 487–489.

8. Marín, A.I.; Rodríguez, J.F.M.; Barberá, J.A.; Fernández-Ortega, J.; Mudarra, M.; Sánchez, D.; Andreo, B. Groundwater vulnerability to pollution in karst aquifers, considering key challenges and considerations: Application to the Ubrique springs in southern Spain. *Hydrogeol. J.* **2021**, *29*, 379–396. [CrossRef]
9. Glassmeyer, S.T.; Furlong, E.T.; Kolpin, D.W.; Cahill, J.D.; Zaugg, S.D.; Werner, S.L.; Meyer, M.T.; Kryak, D.D. Transport of known chemical and microbial compounds in wastewater dischargings: Potential as indicators of human fecal pollution. *Environ. Sci. Technol.* **2005**, *39*, 5157–5169. [CrossRef]
10. Wakida, F.T.; Lerner, D.N. Potential nitrate leaching from groundwater by housing construction. *Int. J. Hydrol. Processes* **2006**, *20*, 2077–2081. [CrossRef]
11. Jiang, C.; Gao, X.; Hou, B.; Zhang, S.; Zhang, J.; Li, C.; Wang, W. Occurrence and environmental impact of coal mine goaf water in karst areas in China. *J. Clean. Prod.* **2020**, *275*, 123813. [CrossRef]
12. Spalding, R.F.; Exner, M.E. The presence of nitrate in groundwater: A review. *J. Environ. Qual.* **1993**, *22*, 392–402. [CrossRef]
13. Aravena, R.; Suzuki, O.; Pena, H.; Pollastri, A.; Fuenzalida, H.; Grilli, A. Isotope composition and genesis of precipitation in northern Chile. *Nucl. Technol.* **1997**, *17*, 103.
14. Moncaster, S.J.; Bottrell, S.H.; Tellam, J.H.; Lloyd, J.W.; Konhauser, K.O. Transport and attenuation of agrochemical pollutants: Implications from sulfate isotope analysis of groundwater. *J. Hydrol. Pollut.* **2000**, *43*, 147–163.
15. Denimal, S.; Tribovillard, N.; Charcoal, F. Leaching and sulfate transfer to chalk aquifers at coal tip (Channel Nord Calais coal Basin, France): An example of acid mine drainage in buffer environments. *Environ. Geol.* **2002**, *42*, 966–981. [CrossRef]
16. Ghiglieri, G.; Barbieri, G.; Vernier, A.; Carletti, A.; Demurtas, N.; Pinna, R.; Pittalis, D. Potential risk of nitrate pollution in aquifers from agricultural practices in the Nula region, Northwestern Sardinia, Italy. *J. Hydrol.* **2009**, *379*, 339–350. [CrossRef]
17. Han, D.; Currell, M.J.; Cao, G. Deep challenges for China's war on water pollution. *Environ. Pollut.* **2016**, *218*, 1222–1233. [CrossRef] [PubMed]
18. Zhou, J.; Xing, L.T.; Zhang, F.J.; Han, Z.; Peng, T.Q.; Xu, M.T.; Yang, Y. Chemical Characteristics Research on Karst Water in Jinan Spring Area. *Adv. Mater. Res.* **2015**, *1092-1093*, 593–596. [CrossRef]
19. Wei, H.; Liang, X.; Liu, S.; Liu, M.; Xiao, C. Hydrochemical Evolution of Groundwater in Dehui, China. *Water* **2020**, *12*, 3378. [CrossRef]
20. Li, S.-L.; Xu, S.; Wang, T.-J.; Yue, F.-J.; Peng, T.; Zhong, J.; Wang, L.-C.; Chen, J.-A.; Wang, S.-J.; Chen, X.; et al. Effects of agricultural activities coupled with karst structures on riverine biogeochemical cycles and environmental quality in the karst region. *Agric. Ecosyst. Environ.* **2020**, *303*, 107120. [CrossRef]
21. Helena, B.; Pardo, R.; Vega, M.; Barrado, E.; Fernandez, J.M.; Fernandez, L. Temporal evolution of groundwater composition in alluvial aquifer (Pisurga River, Spain) based on principal component analysis. *Water Res.* **2000**, *34*, 807–816. [CrossRef]
22. Reghunath, R.; Murthy, T.R.S.; Raghavan, B.R. The utility of multivariate statistical techniques in hydrogeochemical studies: An example from Karnataka, India. *Water Res.* **2002**, *36*, 2437–2442. [CrossRef]
23. Apollaro, C.; Di Curzio, D.; Fuoco, I.; Buccianti, A.; Dinelli, E.; Vespasiano, G.; Castrignano, A.; Rusi, S.; Barca, D.; Figoli, A.; et al. A multivariate non-parametric approach for estimating probability of exceeding the local natural background level of arsenic in the aquifers of Calabria region (Southern Italy). *Sci. Total Environ.* **2022**, *806*, 150345. [CrossRef] [PubMed]
24. Thyne, G.; Guler, C.; Poeter, E. Sequential Analysis of Hydrochemical Data for Watershed Characterization. *Groundwater* **2004**, *42*, 711–723. [CrossRef] [PubMed]
25. Farnham, I.M.; Stetzenbach, K.J.; Singh, A.K.; Johannesson, K.H. Deciphering groundwater flow systems in Oasis Valley, Nevada, using trace element chemistry, multivariate statistics, and geographical information system. *Math. Geol.* **2000**, *32*, 943–968. [CrossRef]
26. Li, B.; Song, X.; Yang, L.; Yao, D.; Xu, Y. Insights onto Hydrologic and Hydro-Chemical Processes of Riparian Groundwater Using Environmental Tracers in the Highly Disturbed Shaying River Basin, China. *Water* **2020**, *12*, 1939. [CrossRef]
27. Glynn, P.; Plummer, L.N. Geochemistry and groundwater system understanding. *J. Hydrogeol.* **2005**, *13*, 263–287. [CrossRef]
28. Jiang, A.; Liu, Yo.; Yi, S.; Guo, Z.; Cui, Y.; Huang, Q.; Li, J.; Liu, K.; Qiu, M.; Jin, X. Impact of artificial recharge on groundwater and springs: Jinan, China, case study. *Arab. J. Geosci.* **2021**, *14*, 111. [CrossRef]
29. Li, F.; Deng, G.; Yuan, J.; Wang, D.; Li, H.; Tang, Y.; Zhou, Y. Study on integrated geophysical method and technology for determining well location of combination of exploration and production: A case study of Wumeng Mountain area. *Prog. Geophys.* **2018**, *33*, 1218–1225.
30. Gao, S.; Li, C.; Jia, C.; Sun, B.; Zhang, H.; Feng, W. Research on chemical characteristics of Baotu Spring Karst water in Jinan. *Acta Geol. Sin.* **2019**, *93*, 61–69.
31. Guo, Y.; Qin, D.; Li, L.; Sun, J.; Li, F.; Huang, J. A Complicated Karst Spring System: Identified by Karst Springs Using Water Level, Hydrogeochemical, and Isotopic Data in Jinan, China. *Water* **2019**, *11*, 947. [CrossRef]
32. Zhu, H.; Xing, L.; Meng, Q.; Xing, X.; Peng, Y.; Li, C.; Li, H.; Yang, L. Water Recharge of Jinan Karst Springs, Shandong, China. *Water* **2020**, *12*, 694. [CrossRef]
33. Chen, Y.; Shu, L.; Li, H.; Opoku, P.A.; Li, G.; Xu, Z.; Qi, T. Identification of Preferential Recharge Zones in Karst Systems Based on the Correlation between the Spring Level and Precipitation: A Case Study from Jinan Spring Basin. *Water* **2021**, *13*, 3048. [CrossRef]
34. Gibbs, R.J. Mechanisms Controlling World Water Chemistry. *Science* **1970**, *170*, 1088–1090. [CrossRef] [PubMed]

35. Chaudhuri, S.; Ale, S. Temporal evolution of groundwater salinity in deep stratified municipal Wells in major aquifers in Texas, USA. *Total Environ. Sci.* **2014**, *472*, 370–380. [CrossRef]
36. Pu, P.; Cao, M.; Zhang, Y.; Yuan, D.; Zhao, H. Hydrochemical indications of human impact on karst groundwater in a subtropical karst area, Chongqing, China. *Environ. Earth Sci.* **2014**, *72*, 1683–1695. [CrossRef]
37. Jebreen, H.; Wohnlich, S.; Banning, A.; Wisotzky, F.; Niedermayr, A.; Ghanem, M. Recharge, geochemical processes and water quality in karst aquifers: Central West Bank, Palestine. *Environ. Earth Sci.* **2018**, *77*, 261. [CrossRef]
38. Xiao, S.; Zeng, C.; Lan, J.; Di, Y.; He, J.; Xiao, H.; Wang, J. Hydrochemical Characteristics and Controlling Factors of Typical Dolomite Karst Basin in Humid Subtropical Zone. *Geofluids* **2021**, *2021*, 8816097. [CrossRef]